# Similarity of Force-Induced Unfolding of Apomyoglobin to Its Chemical-Induced Unfolding: An Atomistic Molecular Dynamics Simulation Approach

Ho Sup Choi, June Huh, and Won Ho Jo
Hyperstructured Organic Materials Research Center, School of Material Science and Engineering, Seoul National University, Seoul 151-742, Korea

ABSTRACT We have compared force-induced unfolding with traditional unfolding methods using apomyoglobin as a model protein. Using molecular dynamics simulation, we have investigated the structural stability as a function of the degree of mechanical perturbation. Both anisotropic perturbation by stretching two terminal atoms and isotropic perturbation by increasing the radius of gyration of the protein show the same key event of force-induced unfolding. Our primary results show that the native structure of apomyoglobin becomes destabilized against the mechanical perturbation as soon as the interhelical packing between the G and H helices is broken, suggesting that our simulation results share a common feature with the experimental observation that the interhelical contact is more important for the folding of apomyoglobin than the stability of individual helices. This finding is further confirmed by simulating both helix destabilizing and interhelical packing destabilizing mutants.

## INTRODUCTION

In the last decade, apomyoglobin has attracted particular interest in both computational and experimental studies of protein folding because it provides important information about the intermediate state of protein folding. From earlier experimental works, it has been known that the apo-form of myoglobin shows three states under acid-induced unfolding with the formation of an intermediate at pH 4 (Hughson et al., 1990, 1991; Barrick and Baldwin, 1993). Intensive NMR studies on apomyoglobin have also revealed that the apomyoglobin has a well-defined native form and its structure is very similar to that of holomyoglobin (Hughson et al., 1990; Jennings and Wright, 1993; Eliezer and Wright, 1996). In addition to these findings, it has been reported that the structure of the molten globule of apomyoglobin has a hydrophobic core associated with helices A, G, and H, whereas the B-helix is largely disordered (Hughson et al., 1990). An experiment for folding kinetics has shown that this molten globular state is on the folding pathway of apomyoglobin (Jennings and Wright, 1993). Subsequently, many experimental works have been focused on early events of the folding to clarify what is the driving force for stabilizing the native and intermediate state of apomyoglobin and for leading to a correct folding (Barrick and Baldwin, 1993; Shin et al., 1993; Sanctis et al., 1994; Ballew et al., 1996; Sabelko et al., 1998). Although many evidences are now integrated to conclude that a portion of GH-helical structure appears first in the early stage of folding of apomyoglobin (Shin et al., 1993; Sabelko et al., 1998), an understanding of the exact role of the G-H hairpin for stability of the protein and its intermediate is far less completed, partly due to lack of information about exact three-dimensional structures of the molten globule and unfolded state.

Recent experiments using the atomic force microscope (AFM) (Rief et al., 1997) and optical tweezer (Kellermayer et al., 1997) have shown that manipulation of single protein molecule is possible and thereby the force needed for unfolding single protein chain is readily measured. By virtue of these experimental developments, an important AFM experiment of protein unfolding has been performed by Rief et al. (1997) who measured the force exerted for unfolding the titin molecule, which maintains the structural integrity of muscle sarcomeres. They recorded the applied force as a function of elongation, where the force required to unfold individual domains ranged from 150 to 300 pN (Rief et al., 1997). Subsequent molecular dynamics simulations have been performed to elucidate the key event of force-induced unfolding of the titin's immunoglobulin domains (Lu et al., 1998; Paci and Karplus, 1999; Lu and Schulten, 2000). The simulation (Lu et al., 1998) has shown that the initial burst of backbone hydrogen bonds between antiparallel $\beta$-strands A and B and between parallel $\beta$-strands A and G leads the maximum force peak.

Although the AFM experiment of a single protein molecule and its corresponding simulation are initiated to study the structural change of proteins with mechanical functions under mechanical perturbation, its significance is not limited to muscle proteins. For proteins whose function is not mechanical such as most of the enzymes, it is also important to characterize the local structure that is essential to the stability of the global structure of the proteins. The question is now whether or not the mechanical unfolding experiment in general can identify the key structural fragments essential to the native form of the protein. It has recently been suggested that mechanical unfolding of a single protein by AFM reflects the same events observed in the

*Submitted December 2, 2002, and accepted for publication May 29, 2003.*
Address reprint requests to Won Ho Jo, Tel.: +82-2-880-7192; Fax: +82-2-885-1748; E-mail: whjpoly@plaza.snu.ac.kr.

0006-3495/03/09/1492/11 $2.00

traditional unfolding experiment (Carrion-Vazquez et al., 1999). As an evidence for this argument, Carrion-Vazquez et al. (1999) indicated that the rate constant of folding and the height of unfolding energy barrier for chemical denaturation are similar to those for AFM unfolding.

There have been other reports that the mechanical unfolding does not follow exactly the pathway of the temperature- or denaturant-induced unfolding (Best et al., 2001; Fowler et al., 2002; Paci and Karplus, 2000). Best et al. (2001) studied the force-induced unfolding of barnase using both AFM and molecular dynamics simulation and showed that unfolding pathways at high temperature differ from the pathways under force. Recently, Fowler et al. (2002) also demonstrated the difference between the force-induced unfolding pathway and the denaturant-induced unfolding pathway in their study of unfolding of an immunoglobulin domain. However, despite the difference in the unfolding pathway, the common features between different unfolding methods have often been reported. Paci and Karplus (2000) have reported that there are common features that indicate the existence of folding cores, although the unfolding pathway of $\beta$-sandwich proteins during stretching simulation is different from that of temperature-induced unfolding.

In the present work, the force-induced unfolding of apomyoglobin is simulated by a molecular dynamics simulation method. One of our primary objectives is to find key structural factors determining the stability of native apomyoglobin and its intermediates identified during mechanical stretching, and to compare the factors to those important for other unfolding methods. To address this, both cases of anisotropic and isotropic mechanical stretching of apomyoglobin are simulated and the results are compared to those of acid-induced unfolding.

## METHODS

Molecular dynamics simulations were performed with the CHARMM program (Brooks et al., 1983). A polar hydrogen model for protein (Neria et al., 1996) and an implicit Gaussian model for solvent (Lazaridis and Karplus, 1999) were used. The initial coordinates were obtained from the x-ray structure of sperm whale myoglobin as deposited in the Brookhaven Protein Data Bank, entry 1BVC (Wagner et al., 1995). The coordinates of the prosthetic group and crystallographic waters were deleted and hydrogen atoms were added. This raw structure of apo-form was energy minimized and gradually heated to 300 K for 100 ps, and then equilibrated further using the Nose-Hoover thermostat (Nose, 1984; Hoover, 1985) for another time span of 1 ns. More than five initial structures were generated by following the above procedure, and the averaged end-to-end distance of the protein was 25.9 Å.

Force-induced unfolding simulations were carried out by two different methods, i.e., distance restraint and constant force restraint. In the distance restraint method, an external force was applied to increase the distance between the N atom of $Val^1$ and the C atom of $Gly^{153}$. In this study, the magnitude of force applied to the two atoms under the harmonic potential is given by

$$|\mathbf{F}| = k|(r_{NC} - r_0)|, \tag{1}$$

where $r_{NC}$ is the distance between the two terminus atoms and $r_0$ is a restraint distance that is increased at a constant rate of 0.5 Å/ps. Constant force restraint was also implemented by applying constant forces of 50 pN, 100 pN, 200 pN, and 300 pN to the two terminus atoms along the vector $\mathbf{r}_{NC}$. All bonds between hydrogen atoms and heavy atoms were fixed using the SHAKE algorithm (Ryckaert et al., 1977), and a time step of 0.002 ps was used.

The simulation with an isotropic bias on the radius of gyration ($R_g$) was executed using the RGYR in the CHARMM program, where the harmonic potential is defined as

$$V = \frac{1}{2}k(R_g - R_g^0)^2, \tag{2}$$

where $k$ is the force constant and $R_g$ is the radius of gyration of the protein, and $R_g^0$ is the restraint distance. The radius of gyration of the protein is defined as

$$R_g^2 = \frac{1}{N}\sum_{i=1}^{N}(\mathbf{r}_i - \mathbf{r}_{cm})^2, \tag{3}$$

where $\mathbf{r}_i$ and $\mathbf{r}_{cm}$ are the position vector of $C_\alpha$ atom and the center of mass of the protein, respectively, and $N$ is the number of residue. In our simulation, a harmonic potential with a force constant of 10 kJ/mol/Å$^2$ is applied to all 153 alpha carbon atoms ($C_\alpha$) of backbone chain, and the restraint distance is increased at a constant rate of 0.005 Å/ps.

The triple mutant (L115A, F123A, and L135A) and the double mutant (N132G and E136G) were generated from the initial structure of the wild type. First, the corresponding side groups of the wild type were replaced with those of mutants, and then the structures of mutants were energy minimized while the position of the backbone chain was constrained to be in the same position as that of the wild type using a harmonic potential. These energy-minimized structures were gradually heated to 300 K for 100 ps and equilibrated for 1 ns using the Nose-Hoover thermostat (Nose, 1984; Hoover, 1985). These final structures are used for the force-induced unfolding simulation of mutants.

## RESULTS

### Characterization of the native state of apomyoglobin

The native structure of apomyglobin is composed of eight helices denoted by alphabetic order from A to H. This native form of apomyoglobin is very similar to that of holomyoglobin except conformational fluctuations in the EF loop, the F-helix, the FG loop, and the beginning of the G-helix (Eliezer and Wright, 1996). Eliezer and Wright (1996) have shown that the A, B, C, D, and E helices are entirely intact and the remainder of G-helix and the first half of H-helix are also intact, when compared to its holo-form. Before mechanical stretching of the protein under study, we have characterized the native state of apomyoglobin using molecular dynamic simulation. The change of helices is plotted as a function of time in Fig. 1, where the helix forming residues are represented by a black dot. The criterion of a residue being ''helical'' or ''not helical'' is based on whether or not the backbone dihedral angles of the given residue are within an appropriate range ($-100° \le \phi \le -30°$ and $-80° \le \psi \le -5°$) and this requirement is met by at least three consecutive residues (Daggett and Levitt, 1992;

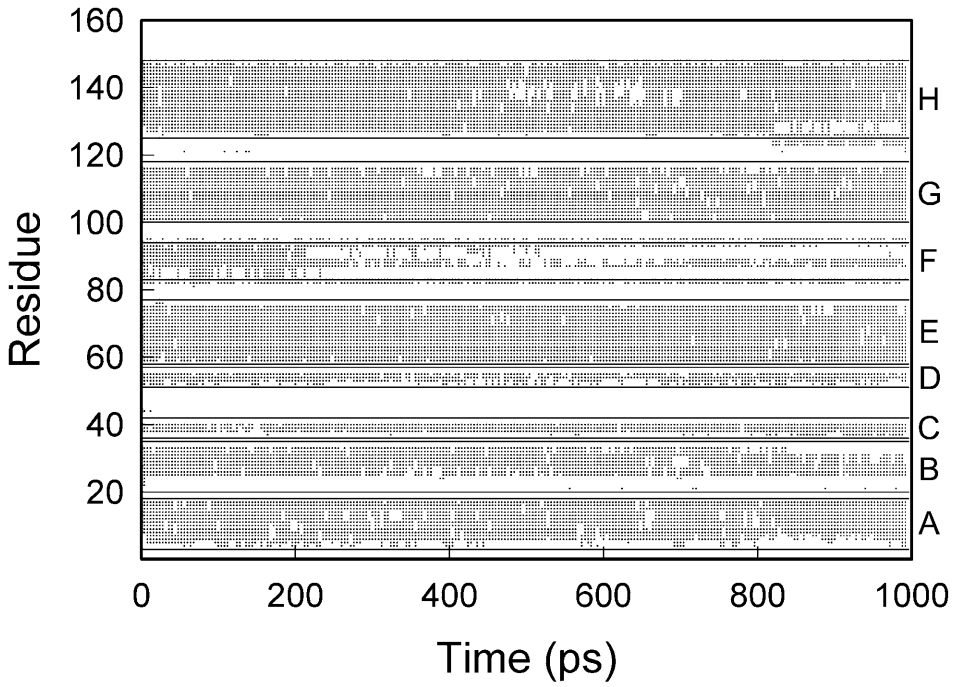


FIGURE 1 The equilibration of the initial structure using the Nose-Hoover thermostat at 300 K for 1 ns. The change of helices with time is plotted every 4 ps by representing the helix forming residue as a black dot. The alphabetical order on the *y* axis of the right side represents the eight helices of apomyoglobin and the solid lines divide the region of each helix.

Tirado-Rives and Jorgensen, 1993). Fig. 1 shows that the A, B, C, D, E, G, and H helices remain almost intact, whereas the F-helix fluctuates significantly and nearly unravels after 200 ps. Although the beginning part of G-helix and the C-terminus of H-helix in simulation shows smaller fluctuation as compared to the experimental observation (Eliezer and Wright, 1996), the root-mean square fluctuation of each residue (data not shown) is very similar to the results from crystallographic B-factor analysis and molecular dynamics simulation using explicit water molecules (Brooks, 1992), and the averaged helix percentage from our simulation is 55.9%, which excellently agrees with the value (55%) measured by circular dichroism (Hughson et al., 1990).

## Force-induced unfolding: distance restraint

To illustrate the mechanical stretching of apomyoglobin, we plot the force-extension profile when the protein is mechanically perturbed. We begin with presenting the profile obtained by the distance restraint method. Fig. 2 represents a $F - r_{NC}$ profile when the pulling speed ($dr_o/dt$) is 0.5 Å/ps. The force profile is obtained by averaging over at least five independent runs. The profile shows a peak at the extension of 150 Å. Thus, the extension of 150 Å can be regarded as the point at which a cooperative unfolding event occurs. After the unfolding event at the extension of 150 Å, the force drops rapidly to 100 pN and then increases slowly, which might be due to the residual structure or the reduction of entropy. This unfolding proceeds until the extension reaches the value for fully extended conformation, i.e., 3 (Å/residue) × 153 (residue) ≅ 450 Å. Beyond 450 Å, the force increases rapidly because the fully extended protein is pulled. Here, it is noted that the maximum force (~250 pN) for apomyoglobin is ~10 times smaller than that for stretching immunoglobulin obtained by Lu et al. (1998). In their work, the immunoglobulin domain consisting of eight

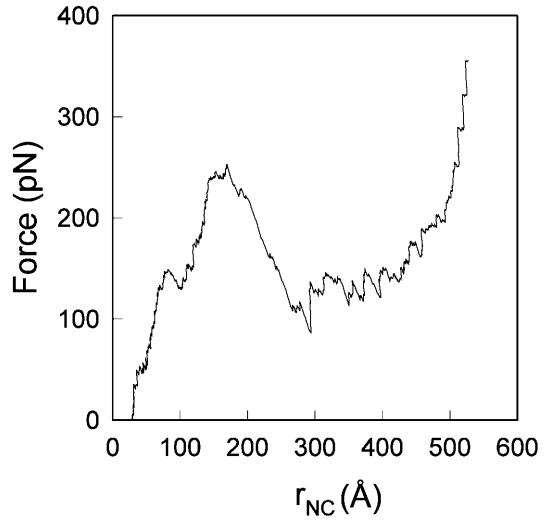


FIGURE 2 The averaged force-extension profile simulated under the distance restraint. The $r_{NC}$ in the plot denotes the distance between the N atom of $Val^1$ and the C atom of $Gly^{153}$. The biasing potential is applied to the two atoms to increase the distance between the two terminal atoms at a stretching rate of 0.5 Å/ps. The averaged end-to-end distance of the initial structure is 25.9 Å.

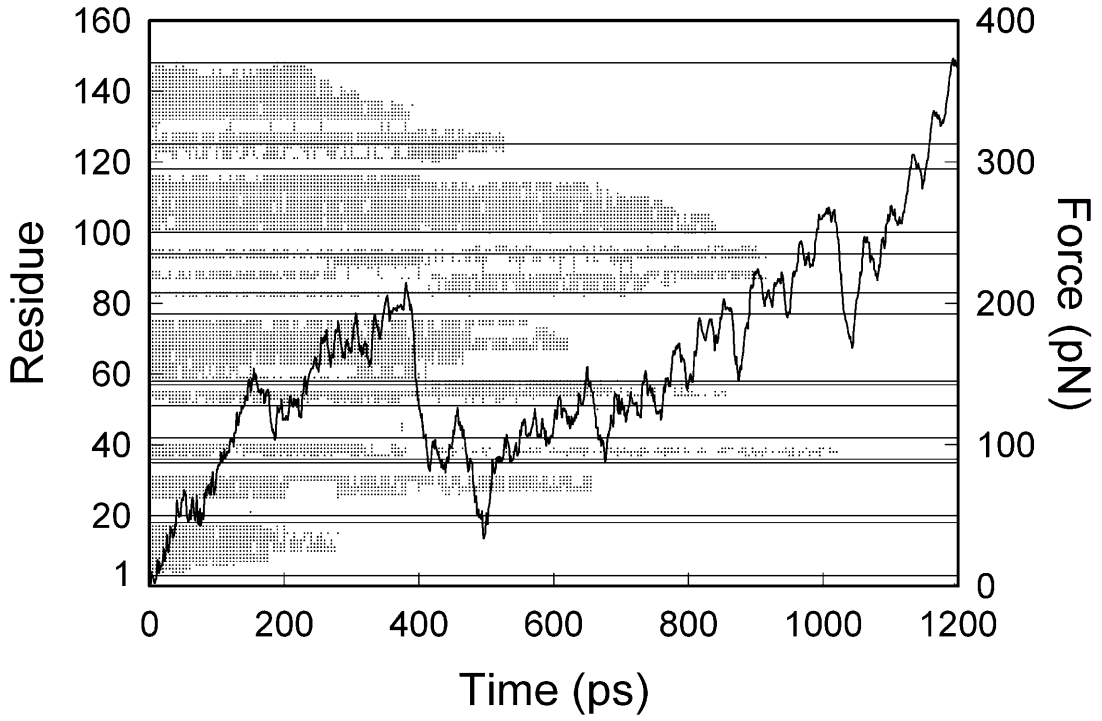


FIGURE 3 The changes of helix structure and external force under the distance restraint with time. The black dots and solid lines in this plot have the same meaning as in Fig. 1.

$\beta$-sheets was pulled at a rate of 0.5 Å/ps and the explicit solvent model was used. The smaller value of force in our simulation seems to be reasonable, because it is known that all-beta proteins in immunoglobulin unfold at higher forces than other proteins.

Because the stability of native apomyoglobin subjected to mechanical stretching becomes critical around the extension of 150 Å, it is necessary to analyze the structural change before and after an extension of 150 Å. In Fig. 3, both the force and the structural change of the helices are plotted against the time elapsed after the stretching is imposed, to establish the relation between the force and the structural change. Fig. 3 shows that the two terminal helices A and H become first unstable after 200 $\sim$ 400 ps and unravel much earlier than other helices. In particular, the A-helix completely unfolds at 300 ps. This can also be confirmed by measuring the solvent accessible surface area of $Trp^7$ and $Trp^{14}$ residues in the A-helix. In the native form, these two residues are buried in the hydrophobic core. Fig. 4 illustrates the solvent accessibility of $Trp^7$ and $Trp^{14}$ as a function of time when the stretching is imposed. The solvent accessibility during stretching is monitored by measuring the surface area exposed to the solvent using the method developed by Lee and Richards (1971). It is clearly seen that both residues become fully exposed to the solvent after 300 ps. Because the hydrophobic core of the native apomyoglobin consists of residues belonging to many different helices, it is conceivable that the unfolding of A-helix having $Trp^7$ and $Trp^{14}$ after 300 ps modifies the packing between A, G, and H helices although some helices are nearly intact after the A-helix unfolds. Fig. 4 also shows that $Trp^7$ is first exposed to solvent while $Trp^{14}$ remains buried in the hydrophobic core until 200 ps, which is comparable to the experimental data (Gulotta et al., 2001).

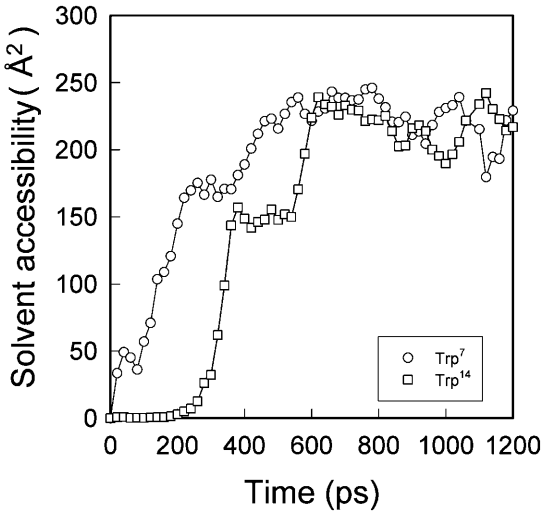


FIGURE 4 The solvent-accessible surface area of $Trp^7$ and $Trp^{14}$ residues in the A-helix. Note that these hydrophobic residues of the A-helix in the native state are buried in the hydrophobic core consisting of the AGH helices.

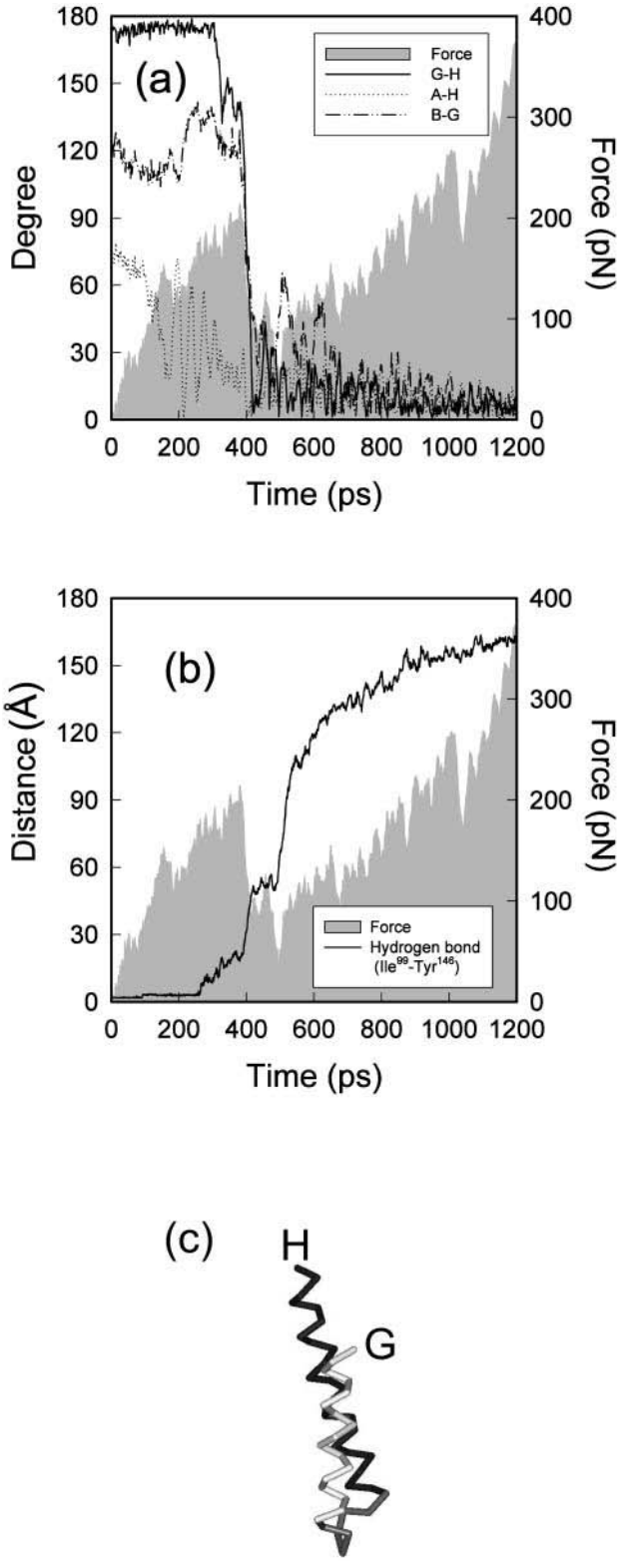


FIGURE 5 The disruption of hydrophobic core. (*a*) The change of external force and axis angles between helices as a function of time during stretching. The axis angle is defined as the angle between the two helices vectors that corresponds to the vector from the N-terminus atom to the C-terminus atom in these two helices. (*b*) Hydrogen bond distance between $Ile^{99}$ in the G-helix and $Tyr^{146}$ in the H-helix. (*c*) The packing between the G (*white*) and H (*black*) helices in the native state. The fragment of the GH hairpin is drawn only using $C_\alpha$ of the backbone chain.

Gulotta et al. (2001) suggested that the initial protection of $Trp^{14}$ as a part of the hydrophobic core lead the concomitant formation of compact secondary and tertiary structures.

The stretching force imposed on two terminal atoms is propagated via peptide linkage and modifies not only the structure inside each helix but also the tertiary structure of the protein, i.e., the interhelical structure. To investigate the change of the tertiary structure under stretching, we measured the axis angles between helices A and H, between G and H and between B and G, as illustrated in Fig. 5 *a*, where the axis angle is defined as the angle between two axes of helices. The force applied to the two terminal atoms is also represented by shaded area. In the native state, these helices contact each other to form a hydrophobic core. Fig. 5 *a* shows that the angles between the A-H helices and between the B-G helices fluctuate even at the early stage of stretching whereas the G-H packing is nearly unchanged until ~300 ps. After ~300 ps when the A-helix is completely unfolded and separated from the hydrophobic core consisting of the A(GH) helices, the interhelical packing between the G and H helices is partly exposed to solvent and becomes slightly unstable. This can be more clearly seen in Fig. 5 *b* where the distance between the residues $Ile^{99}$ (G-helix) and $Tyr^{146}$ (H-helix) that make a hydrogen bond in the native state is plotted against time. The hydrogen bond between these two residues is broken at 300 ps. Because the force still increases until 400 ps (Fig. 5 *a*), the destabilization of the hydrophobic core due to loosening of the A-helix is not the primary determinant of the mechanical unfolding of apomyoglobin. From Fig. 5 *a* alone, one might expect that the BG interhelical structure also sustains until 400 ps because the angle between B and G helical axes is relatively unchanged and rapidly decreases after 400 ps. However, the B-helix partly loses its contacts with the G-helix at 200 ps, whereas the G-helix retains the nativelike contacts with the H-helix, as can be seen in contact map of Fig. 6 *a*. The stable packing between the G and H helices is totally disrupted after 400 ps at which the maximum force is observed (Fig. 5 *a* and Fig. 6 *b*). After 400 ps, the residual interhelical structure does not show any significant resistance to mechanical perturbation, although there are some residual contacts (Fig. 5 *a*, Fig. 6, *b* and *c*). After the cooperative unfolding event, the protein loses nearly all of its nativelike contacts (Fig. 6 *c*). This implies that the critical state of force-induced unfolding of apomyoglobin is closely related to the disruption of hydrophobic core, particularly the stability of the G-H contact.

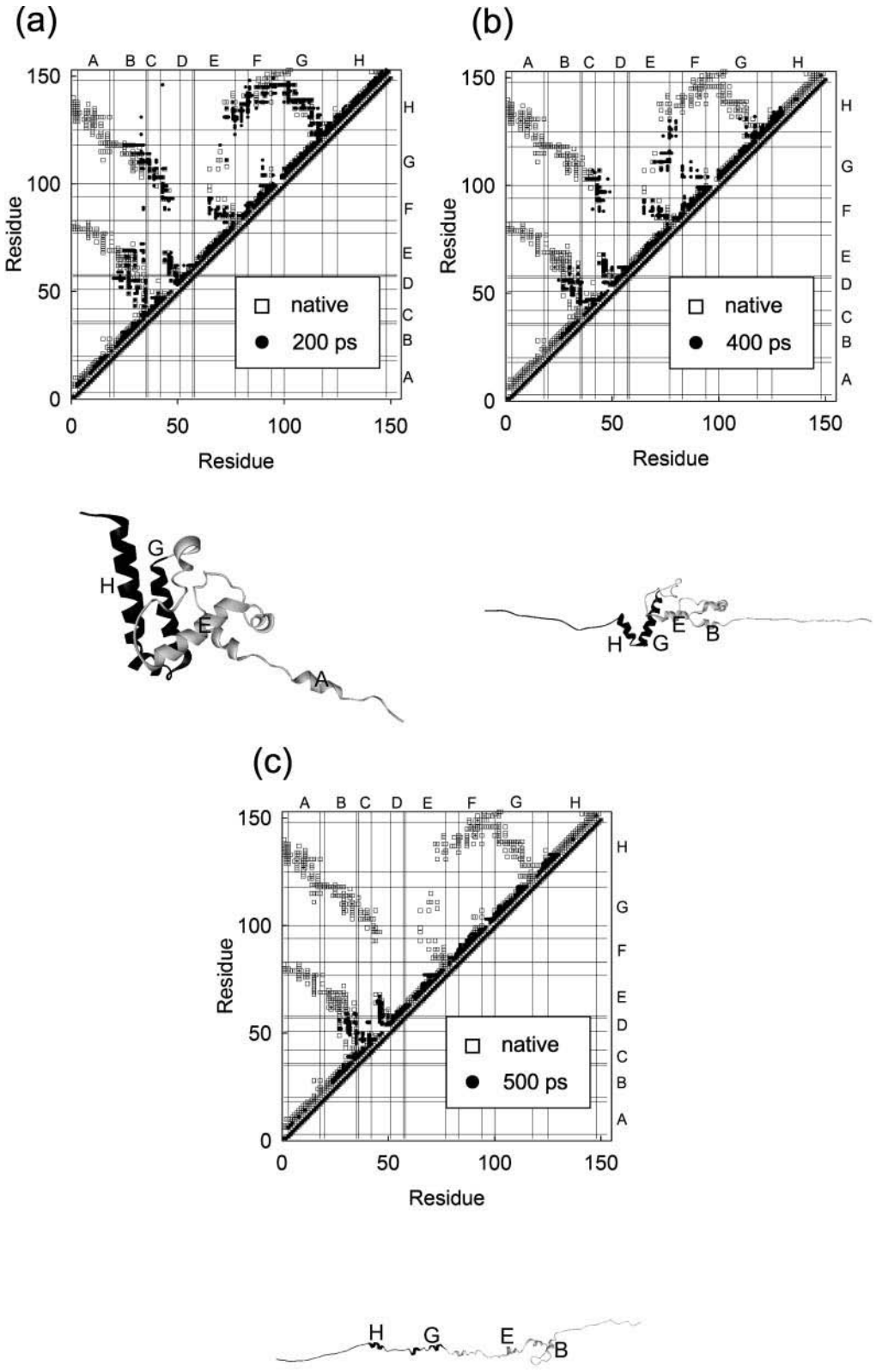


FIGURE 6 The contact maps and their corresponding snapshots of force-induced unfolding of apomyoglobin under distance restraint (*a*) at 200 ps, $r_{NC} = 99$ Å, (*b*) at 400 ps, $r_{NC} = 197$ Å, and (*c*) at 500 ps, $r_{NC} = 268$ Å. In the contact maps, two nonconsecutive residues are considered to make a contact if any side-chain atoms are within 7 Å of each other. For comparison, the contact map for the native state is represented by open squares and those for the snapshot of the force-induced unfolding simulation are represented by filled circles. All snapshots are visualized using WebLab ViewerPro4.0 of Accelrys Inc. (San Diego, CA). In the snapshots, two black ribbons correspond to the G and H helices.

In fact, the side group of an $\alpha$-helix can form ridges that are separated by shallow grooves (Stryer, 1995). Thus, two helices can pack together closely if the ridges of one helix fit into the grooves of the other. In the native state of apomyoglobin, the G and H helices show this type of packing (Fig. 5 *c*). The relative stability of the GH pair observed in Fig. 5 *a* and Fig. 6 *a* might result from the tight packing between the G and H helices.

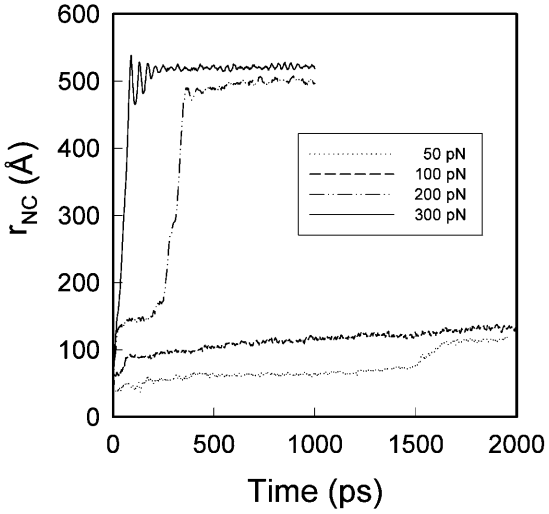


FIGURE 7 The change of end-to-end distance between the N atom of $Val^{1}$ and the C atom of $Gly^{153}$ as a function of time when a constant force is applied to the terminal atoms.

## Force-induced unfolding: constant force restraint

Four values of force, 50 pN, 100 pN, 200 pN, and 300 pN are applied for stretching the apomyoglobin. Apomyoglobin unfolds in a stepwise manner, when it is simulated under constant force condition, as shown in Fig. 7. The extension profile under constant force stretching shows that under the largest constant force (300 pN), the distance ($r_{NC}$) between the two terminus atoms increases very rapidly and reaches the fully extended state without showing any intermediate state. Under the force of 200 pN, the distance $r_{NC}$ increases very rapidly to 150 Å and then remains nearly constant at 150 Å for 200 ps, showing an intermediate state, followed by rapid stretching to the fully extended state. When the force of 100 pN is applied, the distance $r_{NC}$ increases rapidly to 100 Å and then increases gradually to 150 Å, whereas under a mild condition of 50 pN, another intermediate is observed at an extension of ~70 Å.

The structures of these intermediates are illustrated in Fig. 8. Fig. 8 *a* shows that the contact between helices G and H is nearly intact and a part of E-helix is unraveled, whereas other helices are largely disordered. This intermediate state under the constant force of 200 pN is located at 150 Å, which corresponds to the position of the maximum force under distance restraint (Fig. 2). Furthermore, the structure of the intermediate is also very similar to that observed under distance restraint (Fig. 6 *d*), in which the GH helices retain the nativelike contacts whereas the contact between other helices are weakened or almost lost (Fig. 6 *a*). Because 200 pN is slightly less than the maximum force at which the

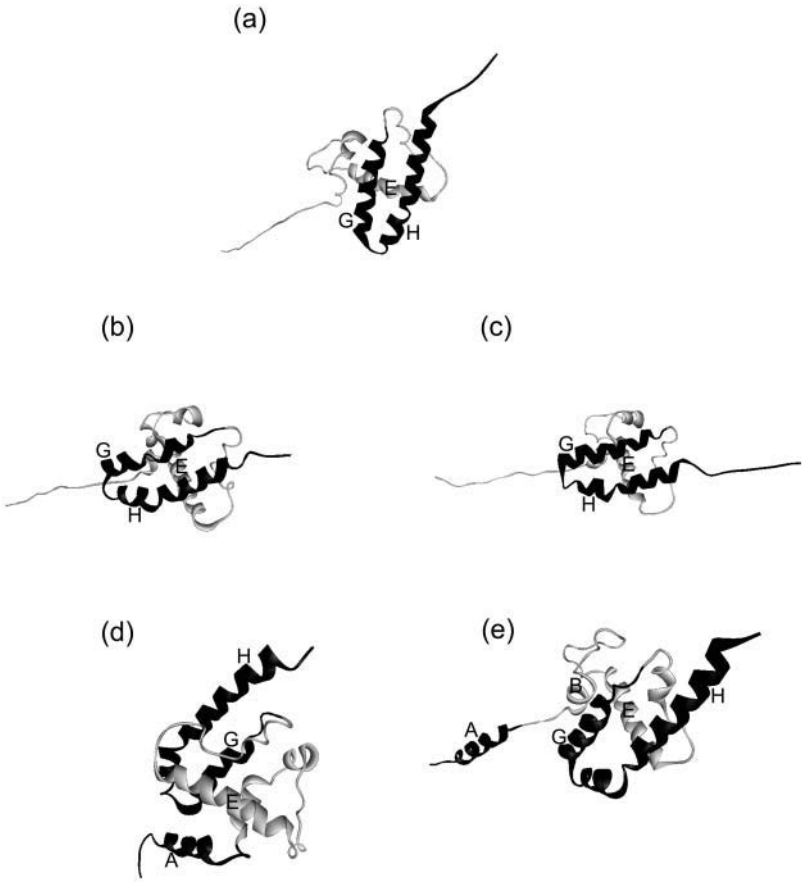


FIGURE 8 Snapshots of force-induced unfolding of apomyoglobin under constant force applied to the N atom of $Val^{1}$ and the C atom of $Gly^{153}$. Two black ribbons correspond to the G and H helices. (*a*) 200 pN, $r_{NC}$ = 143 Å at 100 ps; (*b*) 100 pN, $r_{NC}$ = 117 Å at 1000 ps; (*c*) 100 pN, $r_{NC}$ = 135 Å at 2000 ps; (*d*) 50 pN, $r_{NC}$ = 72 Å at 1400 ps; (*e*) 50 pN, $r_{NC}$ = 103 Å at 1600 ps. All snapshots are visualized using WebLab ViewerPro4.0 of Accelrys Inc.

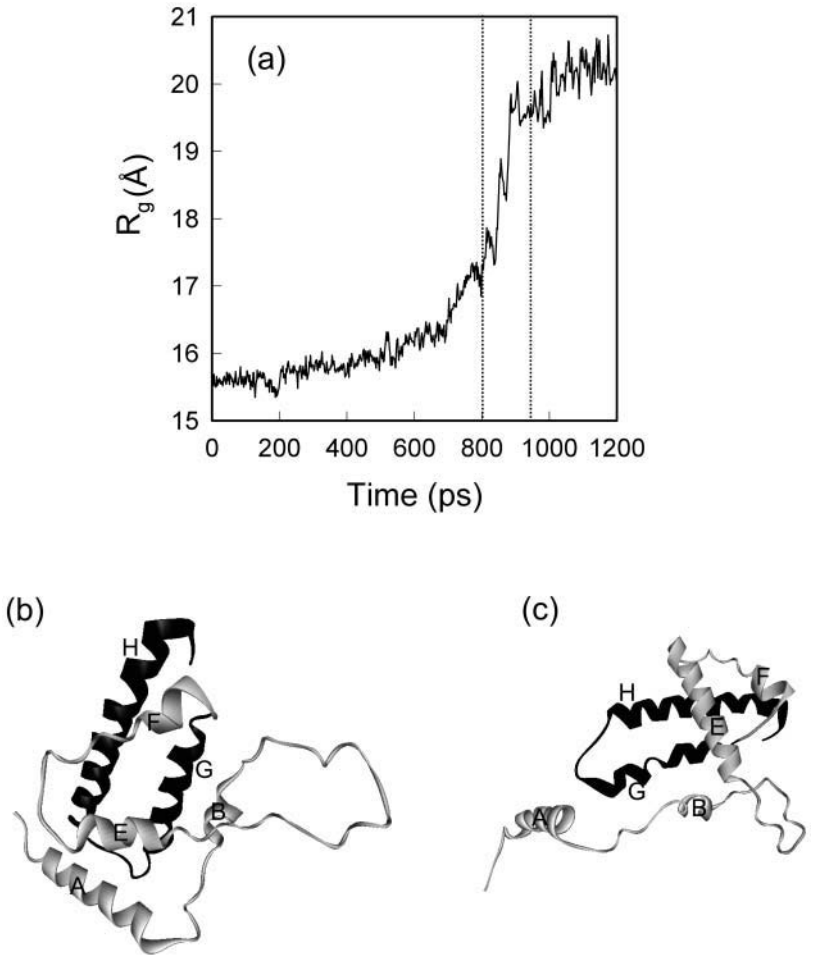


FIGURE 9 Unfolding simulation using a biasing force for increasing the radius of gyration from 16 Å to 21 Å at a constant rate of 0.005 Å/ps. (*a*) The change of the radius of gyration ($R_g$) as a function of time. The dotted lines indicate the region where the value of $R_g$ abruptly increases. (*b*) The snapshot at 800 ps. (*c*) The snapshot at 1200 ps. All snapshots are visualized using WebLab ViewerPro4.0 of Accelrys Inc.

cooperative unfolding occurs (Fig. 5 *a*), the intermediate mainly consisting of the stable GH contacts can be detected under the constant force of 200 pN.

Under a mild condition of 50 pN, the A, G, and H helices are intact as in the native state until an extension of ~70 Å (Fig. 8 *d*), but beyond extension of 100 Å, the A-helix is detached from the hydrophobic core (Fig. 8 *e*), resulting in an intermediate similar to the structure characterized under the constant force of 100 pN or 200 pN. The contact map shows that the A-helix in the native state contacts with the H-helix, the GH loop, the C-terminal of the G-helix, and a part of the E-helix (Fig. 6). Under a stronger force than 100 pN, the A-helix is detached from the hydrophobic core, whereas the GH retain the nativelike contacts with other helices (Fig. 6 *a*). However, under a weak force of 50 pN (Fig. 8 *d*), the A-helix remains in contact with the GH pair. The contact map (data not shown) corresponding to the structure in Fig. 8 *d* shows that under the force of 50 pN, the C-terminal region in the A-helix contacts mainly with both the GH loop and the C-terminal region of the G-helix. This type of motion is also observed indirectly in Fig. 4. In the native state, $Trp^7$ makes contacts with $Ala^{130}$, $Ala^{134}$, and $Leu^{137}$ of the H-helix, and $Trp^{14}$ makes contacts with $Ile^{111}$ and $Leu^{115}$ of the G-helix. In the early stage of the mechanical unfolding, $Trp^7$ loses the contact with the H-helix and is exposed to solvent while $Trp^{14}$ remains buried in the hydrophobic core until 200 ps (Fig. 4).

## DISCUSSIONS

The maximum force under the distance restraint is observed at the position where the GH interhelical packing collapses, as shown in Fig. 5 *a*. The intermediate mainly consisting of the GH helices is also observed under constant force stretching, as shown in Fig. 7 and Fig. 8. This leads us to conclude that a final barrier of force-induced unfolding of apomyoglobin is related to the strong association between the G and H helices.

Because the mechanical stretching by pulling two terminal atoms provides highly anisotropic perturbation to the protein, the unfolding procedure due to the anisotropic stretching may be partly different from other isotropic denaturation method such as pH-induced or solvent-induced denaturation. For instance, the A and H helices of apomyoglobin are known to be nearly intact in the pH-4 intermediate (Hughson et al., 1990), whereas our unfolding simulation of the protein under

anisotropic stretching force shows that the A and H helices become disordered earlier than other helices.

Despite these differences between denaturation methods with respect to the unfolding procedure, our finding that the G-H interhelical packing is the most essential structure for the stability of the native apomyoglobin against anisotropic stretching, as mentioned in the previous section, is consistent with a number of experimental evidences obtained by other denaturation methods. It has been found that the G-H helical hairpin serves as a folding initiation site and leads to stabilization of a folding intermediate (Shin et al., 1993; Sanctis et al., 1994). Moreover, Sabelko et al. (1998) have shown that cold denaturation breaks the AGH-hydrophobic interface of equine apomyoglobin while the G-H helical structure remains intact at the expense of the less stable A-helix. Chi and Asher (1999) have also found that the G and H helices remain intact even at pH 1.5.

These experimental results along with the simulation results in the present study reveal that the G-H interhelical structure of apomyoglobin plays a key role in stabilizing the native form irrespective of denaturation methods. To confirm these findings, we further simulate unfolding of apomyoglobin by applying isotropic stretching force and compared this with the case of anisotropic stretching. The isotropic stretching of the protein is simulated by increasing the radius of gyration ($R_g$) of the protein. Fig. 9 *a* shows the profile of the radius of gyration as a function of time when a harmonic potential is applied to increase the radius of gyration of apomyoglobin molecule. The radius of gyration increases from 16 Å to 21 Å at a constant rate of 0.005 Å/ps. A sharp increase of the radius of gyration is observed between 800 ps and 1000 ps, which implies that a large structural change occurs in the protein. Snapshot pictures (Fig. 9, *b* and *c*) indicates that this abrupt change arises from the detachment of the A-helix from the hydrophobic core consisting of A(GH) helices, while the G-H interhelical packing remains intact. This suggests to us that the intermediate state mainly consisting of the G-H interhelical packing in force-induced unfolding simulation is not a result of an anisotropic perturbation but a generally detected structure irrespective of the unfolding method.

Our simulation results demonstrate that the force-induced unfolding of apomyoglobin arises from the breakdown of contacts between the G and H helices rather than unraveling of A or H helices (Figs. 5 and 6). This implies that the disruption of interhelical packing is a more important factor leading to unfolding of the protein than the destabilization of individual helices. This finding from our force-induced unfolding simulation of apomyoglobin agrees with recent experimental results of apomyoglobin folding (Cavagnero et al., 1999, 2001; Kay et al., 1999). The results showed that the destabilization of H-helix by mutation (N132G and E136G) does not substantially affect either the overall rate of folding or the integrity of the final folded state of apomyoglobin (Cavagnero et al., 1999, 2001). Furthermore, it has been reported that the mutation at helix pairing sites (F123A, L115A, and L135A) decreases the stability and cooperativity of folding of the intermediate, whereas the mutation at hydrophobic residues not involved in interhelical contacts shows little effect on the stability or cooperativity (Kay et al., 1999). To examine whether our force-induced unfolding simulation can predict the effect of mutation on the stability and cooperativity of folding of the intermediate, we have simulated the force-induced unfolding of mutants under the constant force of 200 pN applied to the N atom of $Val^1$ and the C atom of $Gly^{153}$. The intermediate detected at 150 Å under the constant force of 200 pN is largely disordered by mutations at helix pairing sites (L115A, F123A, and L135A), whereas the H-helix destabilizing mutation (N132G and E136G) does not affect the stability of intermediate significantly (Fig. 10). Therefore, it is concluded that our force-induced unfolding simulation properly reflects those experimental observations that the interhelical packing is more important for folding of apomyoglobin than individual helices.

In this paper, we have investigated the relationship between force-induced unfolding and traditional unfolding using apomyoglobin as a model protein. Recent force-induced unfolding simulation of $\beta$-hairpin fragment of protein G has shown that the unfolding pathway depends on the pulling speed (Bryant et al., 2000). However, the results of our simulation for unfolding of apomyoglobin share the common feature with that of the traditional unfolding experiment, although the high pulling speed adopted in our force-induced unfolding simulation may lead to a change of unfolding pathway because the A and H helices are destabilized earlier than other helices. In fact,

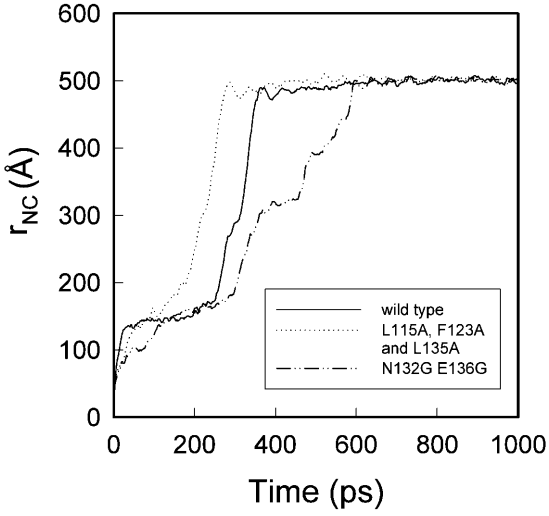


FIGURE 10 Force-induced unfolding for two types of mutants under the constant force of 200 pN applied to the N atom of $Val^1$ and the C atom of $Gly^{153}$. The mutation at L115A, F123A, and L135A is used for destabilizing interhelical packing and the mutation at N132G and E136G is used for destabilizing H-helix.

Paci and Karplus (2000) have shown that there are common features that indicate the existence of folding cores for $\beta$-sandwich proteins, although the results of stretching simulations are different from those of temperature-induced unfolding. In the case of apomyoglobin, Cavagnero et al. (2001) have also shown that apomyoglobin is capable of compensating for mutations destabilizing the H-helix by following alternative folding pathways within a common basic framework. These evidences support that the folding or unfolding pathway can change without altering the structure of the intermediate.

We have shown that force-induced unfolding is a very useful method for studying the structural change of protein whose function is not mechanical. Basically, it is very difficult to simulate pH-induced unfolding or solvent-induced unfolding due to the limited timescale and the absence of an appropriate force field. However, force-induced unfolding simulation is computationally efficient for analyzing protein unfolding, because it can accelerate the unfolding process by facilitating escape from local minima in a rugged free energy landscape of protein folding. If the force-induced unfolding is combined with more delicate methods such as $\Phi$-value analysis (Fersht, 1999; Best et al., 2002), the method can provide more detail information about the transition state of protein folding and deduce the folding pathway by reversing the unfolding process.

The authors thank the Korea Science and Engineering Foundation (KOSEF) for financial support through the Hyperstructured Organic Materials Research Center (HOMRC). One of the authors (J. Huh) thanks the Ministry of Education, the Republic of Korea for its financial support through the BK21 program.

## REFERENCES

Ballew, R. M., J. Sabelko, and M. Gruebele. 1996. Direct observation of fast protein folding: the initial collapse of apomyoglobin. *Proc. Natl. Acad. Sci. USA*. 93:5759–5764.

Barrick, D., and R. L. Baldwin. 1993. Three-state analysis of sperm whale apomyoglobin folding. *Biochemistry*. 32:3790–3796.

Best, R. B., B. Li, A. Steward, V. Daggett, and J. Clarke. 2001. Can non-mechanical proteins withstand force? Stretching barnase by atomic force microscopy and molecular dynamics simulation. *Biophys. J*. 81:2344–2356.

Best, R. B., S. B. Fowler, J. L. Toca-Herrera, and J. Clarke. 2002. A simple method for probing the mechanical unfolding pathway of proteins in detail. *Proc. Natl. Acad. Sci. USA*. 99:12143–12148.

Brooks, B. R., R. E. Bruccoleri, B. D. Olafson, D. J. States, S. Swaminathan, and M. Karplus. 1983. CHARMM: a program for macromolecular energy, minimization and dynamics calculations. *J. Comput. Chem*. 4:187–217.

Brooks, C. L. 1992. Characterization of native apomyoglobin by molecular dynamics simulation. *J. Mol. Biol*. 227:375–380.

Bryant, Z., V. S. Pande, and D. S. Rokhsar. 2000. Mechanical unfolding of a $\beta$-hairpin using molecular dynamics. *Biophys. J*. 78:584–589.

Carrion-Vazquez, M., A. F. Oberhauser, S. B. Fowler, P. E. Marazalek, S. E. Broedel, J. Clarke, and J. M. Fernandez. 1999. Mechanical and chemical unfolding of a single protein: a comparison. *Proc. Natl. Acad. Sci. USA*. 96:3694–3699.

Cavagnero, S., H. J. Dyson, and P. E. Wright. 1999. Effect of H helix destabilizing mutations on the kinetic and equilibrium folding of apomyoglobin. *J. Mol. Biol*. 285:269–282.

Cavagnero, S., C. Nishimura, S. Schwarzinger, H. J. Dyson, and P. E. Wright. 2001. Conformational and dynamic characterization of the molten globule state of an apomyoglobin mutant with an altered folding pathway. *Biochemistry*. 40:14459–14467.

Chi, Z., and S. A. Asher. 1999. Ultraviolet resonance Raman examination of horse apomyoglobin acid unfolding intermediates. *Biochemistry*. 38:8196–8203.

Daggett, V., and M. Levitt. 1992. Molecular dynamics simulations of helix denaturation. *J. Mol. Biol*. 223:1121–1138.

Eliezer, D., and P. E. Wright. 1996. Is apomyoglobin a molten globule? Structural characterization by NMR. *J. Mol. Biol*. 263:531–538.

Fersht, A. 1999. Structure and Mechanism in Protein Science. W. H. Freeman and Company, New York.

Fowler, S. B., R. B. Best, J. L. Toca-Herrera, T. J. Rutherford, A. Steward, E. Paci, M. Karplus, and J. Clarke. 2002. Mechanical unfolding of a titin Ig domain: structure of unfolding intermediate revealed by combining AFM, molecular dynamics simulations, NMR and protein engineering. *J. Mol. Biol*. 322:841–849.

Gulotta, C., R. Gilmanshin, T. C. Buscher, R. H. Callender, and R. B. Dyer. 2001. Core formation in apomyoglobin: probing the upper reaches of the folding energy landscape. *Biochemistry*. 40:5137–5143.

Hoover, W. G. 1985. Canonical dynamics: equilibrium phase-space distributions. *Phys. Rev. A*. 31:1695–1697.

Hughson, F. M., D. Barrick, and R. L. Baldwin. 1991. Probing the stability of a partly folded apomyoglobin intermediate by site-directed mutagenesis. *Biochemistry*. 30:4113–4118.

Hughson, F. M., P. E. Wright, and R. L. Baldwin. 1990. Structural characterization of a partly folded apomyoglobin intermediate. *Science*. 249:1544–1548.

Jennings, P. A., and P. E. Wright. 1993. Formation of a molten globule intermediate early in the kinetic folding pathway of apomyoglobin. *Science*. 262:892–896.

Kay, M. S., C. H. I. Ramos, and R. L. Baldwin. 1999. Specificity of native-like interhelical hydrophobic contacts in the apomyoglobin intermediate. *Proc. Natl. Acad. Sci. USA*. 96:2007–2012.

Kellermayer, M., S. Smith, H. Granzier, and C. Bustamante. 1997. Folding-unfolding transition in single titin modules characterized with laser tweezers. *Science*. 276:1112–1116.

Lazaridis, T., and M. Karplus. 1999. Effective energy function for protein dynamics and thermodynamics. *Proteins Struct. Funct. Genet*. 35:133–152.

Lee, B., and F. M. Richards. 1971. The interpretation of protein structures: estimation of static accessibility. *J. Mol. Biol*. 55:379–400.

Lu, H., B. Isralewitz, A. Krammer, V. Vogel, and K. Schulten. 1998. Unfolding of titin immunoglobulin domains by steered molecular dynamics simulation. *Biophys. J*. 75:662–671.

Lu, H., and K. Schulten. 2000. The key event in force-induced unfolding of titin's immunoglobulin domains. *Biophys. J*. 79:51–65.

Neria, E., S. Fischer, and M. Karplus. 1996. Simulation of activation free energies in molecular dynamics system. *J. Chem. Phys*. 105:1902–1921.

Nose, S. 1984. A molecular dynamics method for simulations in the canonical ensemble. *Mol. Phys*. 52:255–268.

Paci, E., and M. Karplus. 1999. Forced unfolding of fibronectin type 3 modules: an analysis by biased molecular dynamics simulation. *J. Mol. Biol*. 288:441–459.

Paci, E., and M. Karplus. 2000. Unfolding proteins by external forces and temperature: the importance of topology and energetics. *Proc. Natl. Acad. Sci. USA*. 97:6521–6526.

Rief, M., M. Gautel, F. Oesterhelt, J. M. Fernandez, and H. E. Gaub. 1997. Reversible unfolding of individual titin immunoglobulin domains by AFM. *Science*. 276:1109–1112.

Ryckaert, J. P., G. Ciccotti, and H. J. C. Berendsen. 1977. Numerical integration of the Cartesian equations of motion of a system with constraints: molecular dynamics of *n*-alkanes. *J. Comp. Phys.* 23:327–341.

Sabelko, J., J. Ervin, and M. Gruebele. 1998. Cold-denatured ensemble of apomyoglobin: implications for the early steps of folding. *J. Phys. Chem.* 102:1806–1819.

Sanctis, G. D., F. Ascoli, and M. Brunori. 1994. Folding of apominimyoglobin. *Proc. Natl. Acad. Sci. USA.* 91:11507–11511.

Shin, H. C., G. Merutka, J. P. Waltho, L. L. Tennant, H. J. Dyson, and P. E. Wright. 1993. Peptide models of proteins folding initiation sites. 3. The G-H helical hairpin of myoglobin. *Biochemistry.* 32:6356–6364.

Stryer, L. 1995. Biochemistry, 4th ed. W. H. Freeman and Company, New York. 423–424.

Tirado-Rives, J., and W. L. Jorgensen. 1993. Molecular dynamics simulations of the unfolding of apomyoglobin in water. *Biochemistry.* 32:4175–4184.

Wagner, U. G., N. Moeiler, W. Schmitzberger, H. Falk, and C. Kratky. 1995. Structure determination of the biliverdin apomyoglobin complex: crystal structure analysis of two crystal forms at 1.4- and 1.5-Å resolution. *J. Mol. Biol.* 247:326–337.